Viscoelastic turbulent boundary layer with near-wall injection of polymer molecules

By M. Shin AND E. S. G. Shaqfeh

1. Motivation and objectives

In 1948, B. A. Toms reported that small amount of long-chain polymer molecules can dramatically reduce drag in turbulent pipe flows. After this observation, there have been extensive studies on this phenomenon. To explain the mechanism of turbulent drag reduction, three different hypotheses were suggested by Lumley (1969, 1973), Tabor & de Gennes (1986), and Joseph (1990). Lumley (1969) suggested that the drag reduction occurs when the polymer relaxation time λ is longer than a characteristic time scale of near-wall turbulence:

$$\lambda > \nu/{u_\tau}^2\,, \tag{1.1}$$

where ν is the kinematic viscosity of polymeric solution and u_τ is the friction velocity defined from the wall shear stress. In addition to this, Lumley (1973) conjectured that the coil-stretch transition of polymer molecules may induce a huge increase in elongational viscosity, and thereby the drag may be reduced. Tabor & de Gennes (1986) proposed the elastic theory, in which the turbulence cascade in the region of high wave numbers may be prohibited by the polymer molecules absorbing the energy of small-scale turbulence, and they suggested that the drag reduction may occur before polymers injected into the core of the pipe reach the wall. Joseph (1990) supposed that the the polymer molecules attenuate the small-scale turbulence so that there exists a cut-off scale represented by the shear wave speed u_c. Thereby, he suggested the following criterion for drag reduction:

$$u_\tau > u_c \equiv (\nu/\lambda)^{1/2}\,. \tag{1.2}$$

To resolve this unsolved issue, many experimental and numerical studies have been conducted, and the brief reviews of those works can be found in the relatively recent works of Min *et al.* (2003) and Dubief *et al.* (2004). Based on the numerical experiments for the fully developed viscoelastic turbulent channel flows with uniform polymer concentrations, which were developed originally by Sureshkumar *et al.* (1997), Min *et al.* (2003) and Dubief *et al.* (2004) suggest the following different scenarios for the drag-reduction mechanism.

Min *et al.*'s scenario: "When drag reduction occurs the turbulent kinetic energy near the wall is absorbed by the polymer and transformed into elastic energy. This elastic energy near the wall is lifted up by the near-wall vortical motion and released as turbulent kinetic energy or is dissipated in the buffer and log layers."

Dubief *et al.*'s scenario: "Polymers are stretched mainly by straining motion around vortices (store energy) and re-coiled in the near-wall region (release energy), resulting in the vortex damping in $y^+ > 20$ and the enhancement of near-wall streaks in $y^+ < 20$."

Until now, the numerical approaches based on the elastic theory have been based on the assumption that the polymer molecules are distributed homogeneously in space and, therefore the rheological parameters such as solvent viscosity, polymer viscosity

and polymer relaxation time can be fixed at constant values throughout the domain for a certain concentration of polymer molecules. Even though the existing numerical experiments revealed many sides of the drag-reducing mechanism, the interaction between the turbulence and the polymer molecules is still unclear in these types of homogeneous approaches. There is a need to investigate the viscoelastic turbulence in the near-wall region with spatially inhomogeneous concentration of polymers.

The objective of the present work is to investigate the interaction between turbulence and the presence of polymer molecules non-uniformly distributed in space. The finite extensible, nonlinear elastic, pre-averaged (FENE-P) dumbbell model is adopted to represent the coil-stretch behavior of polymer molecules in micro-state. Since the concentration of polymer molecules is spatially non-uniform, the rheological parameters such as solvent viscosity η_s, polymer viscosity η_p, and polymer relaxation time λ need to be specified as a function of polymer concentration by utilizing the rheological data of PEO polymer molecules modeled as FENE-P dumbbells. In this work, 500 to 1000 [ppm] of polymer molecules are injected at very-near the wall on the inflow plane. From this specific configuration of polymer injection, we are going to see which kinds of drag-reduction regimes (low-drag reduction, high-drag reduction, or maximum-drag reduction) occur and are going to try to explain the drag reduction mechanism by introducing a new time scale of transit time of near-wall polymer molecules and a polymer shear viscosity induced by the polymer shear stress. The transit time will be defined as a time scale during which the stretched polymer molecules travel to the buffer layer, in which the coherent vortical motion is dominant, and the polymer shear viscosity will be defined to represent an additional viscous dissipation due to the polymer molecules.

2. Governing equations and rheologies

The viscoelastic motion of polymeric solution with spatially inhomogeneous concentration of polymer molecules may be described by the following set of equations:

$$\rho\left(\frac{\partial \tilde{\boldsymbol{u}}}{\partial \tilde{t}} + \tilde{\boldsymbol{u}}\cdot\tilde{\nabla}\tilde{\boldsymbol{u}}\right) = -\tilde{\nabla}\tilde{p} + \tilde{\nabla}\cdot\left(2\eta_s\,\tilde{\boldsymbol{S}} + \tilde{\boldsymbol{\tau}}_p\right) \tag{2.1}$$

$$\tilde{\nabla}\cdot\tilde{\boldsymbol{u}} = 0 \tag{2.2}$$

$$\frac{\partial \boldsymbol{c}}{\partial \tilde{t}} + \tilde{\boldsymbol{u}}\cdot\tilde{\nabla}\boldsymbol{c} = \boldsymbol{c}\cdot\tilde{\nabla}\tilde{\boldsymbol{u}} + \left(\boldsymbol{c}\cdot\tilde{\nabla}\tilde{\boldsymbol{u}}\right)^{\top} - \frac{1}{\lambda}(f\boldsymbol{c} - \boldsymbol{I}) \tag{2.3}$$

$$\frac{\partial C}{\partial \tilde{t}} + \tilde{\boldsymbol{u}}\cdot\tilde{\nabla}C = D\,\tilde{\nabla}^2 C\,, \tag{2.4}$$

where ρ is the density of polymeric solution, $\tilde{\boldsymbol{u}}$ the velocity vector of polymeric solution, $\tilde{p}$ the hydrodynamic pressure, C the concentration of polymer molecules, $\boldsymbol{S}$ the rate-of-strain tensor,

$$\tilde{\boldsymbol{S}} = \frac{1}{2}\left(\tilde{\nabla}\tilde{\boldsymbol{u}} + \tilde{\nabla}\tilde{\boldsymbol{u}}^{\top}\right),$$

$\boldsymbol{\tau}_p$ the polymer stress,

$$\tilde{\boldsymbol{\tau}}_p = \frac{\eta_p}{\lambda}\left(f\boldsymbol{c} - \boldsymbol{I}\right),$$

$f(\equiv \frac{1}{1-c_{kk}/L^2})$ the Peterlin function, $\boldsymbol{c}$ the conformation tensor (diadic tensor composed of end-to-end vector of polymer), c_{kk} the trace of the conformation tensor, L the maximum stretched length of polymer molecule, D the molecular diffusion coefficient of

polymers concentration, and the tilde mark in the equations denotes the dimensional quantities. The conformation tensor $\boldsymbol{c}$ is dimensionless with respect to k_BT/H, where k_B, T and H denote the Boltzmann constant ($k_B = 1.38 \times 10^{-23}$ [J/K]), the absolute temperature, and the dumbbell spring constant, respectively. As the rheological properties of the polymeric flows, η_s is the solvent viscosity, η_p is the zero-shear polymer viscosity, and λ is the polymer relaxation time.

2.1. *Non-dimensionalization of equations*

U_{fs} and l_c are chosen to be the characteristic velocity and length scales, respectively, by replacing the dimensional quantities in the above equations with following non-dimensional ones:

$$\tilde{t} = t\, l_c/U_{fs}\,,\ \tilde{\boldsymbol{u}} = \boldsymbol{u}\, U_{fs}\,,\ \tilde{\nabla} = \nabla/l_c\,,\ \tilde{p} = p/\rho {U_{fs}}^2\,,\ \tilde{\boldsymbol{\tau}}_p = \boldsymbol{\tau}_p/\rho {U_{fs}}^2\,,\ C = \phi C^*\,.$$

The governing equations for the viscoelastic fluid are rewritten as

$$\frac{\partial \boldsymbol{u}}{\partial t} + \boldsymbol{u}\cdot\nabla\boldsymbol{u} = -\nabla p + \nabla\cdot\boldsymbol{\tau} \tag{2.5}$$

$$\boldsymbol{\tau} = \frac{1}{Re}\frac{\eta_s(\phi)}{\eta_{s0}}\big(\nabla\boldsymbol{u} + \nabla\boldsymbol{u}^\top\big) + \frac{1}{Re}\frac{\eta_p(\phi)}{\eta_{s0}}\frac{1}{We(\phi)}\big(f\boldsymbol{c} - \boldsymbol{I}\big) \tag{2.6}$$

$$\nabla\cdot\boldsymbol{u} = 0 \tag{2.7}$$

$$\frac{\partial \boldsymbol{c}}{\partial t} + \boldsymbol{u}\cdot\nabla\boldsymbol{c} = \boldsymbol{c}\cdot\nabla\boldsymbol{u} + \big(\boldsymbol{c}\cdot\nabla\boldsymbol{u}\big)^\top - \frac{1}{We(\phi)}(f\boldsymbol{c} - \boldsymbol{I}) \tag{2.8}$$

$$\frac{\partial\,\phi}{\partial t} + \boldsymbol{u}\cdot\nabla\,\phi = \frac{1}{Re\,Sc}\,\nabla^2\,\phi\,, \tag{2.9}$$

where η_{s0} is the viscosity of pure solvent (water), $Re = \rho U_{fs} l_c/\eta_{s0}$ the Reynolds number based on a characteristic length, $We = \lambda U_{fs}/l_c$ the Weissenberg number, and $Sc = \eta_{s0}/\rho D$ the Schmidt number for the polymer concentration.

2.2. *Polymeric solution with concentration-dependent rheologies*

If the concentration of polymer molecules is spatially inhomogeneous in the solution, the rheological properties of the polymer solution need to be considered as a function of the concentration of polymer molecules. Since the polymer concentration C is the function of position, η_p, η_s and λ are not constant, but rather they vary spatially. Precisely speaking, the rheologies of polymeric solution depend on the shear rate as well as on the concentration of polymer molecules. In the present work, the low shear values of the rheologies will be used to prepare the concentration-dependent rheologies, in which the shear-thinning effects occurred at the high-shear region will be neglected. The effect of the polymer concentration can be fitted into the following forms of the rheologies by utilizing the experimental data at the low-shear region for the PEO polymers modelled as FENE-P dumbbells (*WSR301 MI series*):

$$\eta_s = \eta_{s0}\big(1 + \phi^{1.2}\big) = \eta_{s0}\mathcal{M}_s(\phi) \tag{2.10}$$

$$\eta_p = n(C)kT\lambda_0\big(1 + 0.6235\,\phi^{2.2}\big) = \eta_{s0}\mathcal{M}_p(\phi) \tag{2.11}$$

$$\lambda = \lambda_0 + 0.4351\,\phi^{0.7}\big(1 + 0.885\,\phi\big) = \lambda_0\mathcal{L}(\phi)\,, \tag{2.12}$$

where n is the number of molecules per unit volume. For the PEO polymer molecules, the molecular weight is around $4{\times}10^6$ [Da] $= 6.64{\times}10^{-21}$ [kg]. Since 1 [ppm] equals to $1{\times}10^{-3}$

[kg/m^3], the polymer concentration C [ppm] equals to $1.506 \times 10^{17} C$ [molecules/m^3]; i.e. $n = 1.506 \times 10^{17} C$. For water at standard conditions ($T = 300$ [K]), the viscosity of pure solvent $\eta_{s0} = 1 \times 10^{-3}$ [Pa], and the polymer relaxation time in the limit of dilute regime of polymer molecules, λ_0 (we call it 'Zimm time'), is 1.23×10^{-3} [sec.]. The concentration parameter, ϕ, denotes the polymer concentration normalized with a certain critical concentration, $C^* = 590$ [ppm], at which the hydrodynamic or mechanical interactions between polymer molecules begin to be significant. The concentration-dependent functions can be expressed in terms of $\phi \equiv C/C^*$:

$$\mathcal{M}_s(\phi) = 1 + \phi^{1.2} \tag{2.13}$$

$$\mathcal{M}_p(\phi) = 0.4525\,\phi\big(1 + 0.6235\,\phi^{2.2}\big) \tag{2.14}$$

$$\mathcal{L}(\phi) = 1 + 353.7\,\phi^{0.7}\big(1 + 0.885\,\phi\big)\,. \tag{2.15}$$

The Weissenberg number is the function of polymer concentration:

$$We(\phi) = We_0 \mathcal{L}(\phi)\,,$$

where $We_0 = \lambda_0 U_{fs}/l_c$. The hydrodynamic stress in the polymeric solution is composed of the contributions by solvent and polymers; $\boldsymbol{\tau} = \boldsymbol{\tau}_s + \boldsymbol{\tau}_p$. The solvent stress $\boldsymbol{\tau}_s$ is

$$\boldsymbol{\tau}_s = \frac{2}{Re}\mathcal{M}_s(\phi)\boldsymbol{S}$$

and the polymer stress $\boldsymbol{\tau}_p$ is

$$\boldsymbol{\tau}_p = \frac{1}{Re}\frac{\mathcal{M}_p(\phi)}{We_0\,\mathcal{L}(\phi)}(f\boldsymbol{c} - \boldsymbol{I})\,.$$

From these separate contributions, we can readily determine the fact that as the concentration of polymers goes down, the polymer stress contribution is weakened and finally vanishes, since $\mathcal{M}_p(\phi)$ goes to zero as ϕ decreases to zero. The viscosity ratio β is defined as

$$\beta \equiv \frac{\eta_s}{\eta_s + \eta_p} = \frac{\mathcal{M}_s(\phi)}{\mathcal{M}_s(\phi) + \mathcal{M}_p(\phi)}\,.$$

In the previous numerical experiments for the viscoelastic turbulent flows containing spatially homogeneous polymer molecules, the viscosities of η_s and η_p were constant and the parameter β was chosen to be an arbitrary value less than unity to get a viscoelasticity.

2.3. *Momentum equation and friction velocity*

From (2.5), the instantaneous momentum equation can be expressed as

$$\frac{\partial \boldsymbol{u}}{\partial t} + \boldsymbol{u}\cdot\nabla\boldsymbol{u} = -\nabla p + \nabla\cdot\boldsymbol{\tau}_s + \nabla\cdot\boldsymbol{\tau}_p\,. \tag{2.16}$$

Taking the Reynolds decompositions,

$$\boldsymbol{u} = \boldsymbol{U} + \boldsymbol{u}',\ p = P + p',\ \boldsymbol{\tau}_s = \bar{\boldsymbol{\tau}}_s + \boldsymbol{\tau}_s',\ \boldsymbol{\tau}_p = \bar{\boldsymbol{\tau}}_p + \boldsymbol{\tau}_p',$$

mean momentum equation is obtained as

$$\frac{\partial \boldsymbol{U}}{\partial t} + \boldsymbol{U}\cdot\nabla\boldsymbol{U} = -\nabla P + \nabla\cdot\Big(-\overline{\boldsymbol{u}'\boldsymbol{u}'} + \bar{\boldsymbol{\tau}}_s + \bar{\boldsymbol{\tau}}_p\Big)\,. \tag{2.17}$$

The total shear stress τ_{xy} is defined from the axial-momentum equation (2.17):

$$\tau_{xy} = -\overline{u'v'} + \bar{\tau}_{s,xy} + \bar{\tau}_{p,xy}\,. \tag{2.18}$$

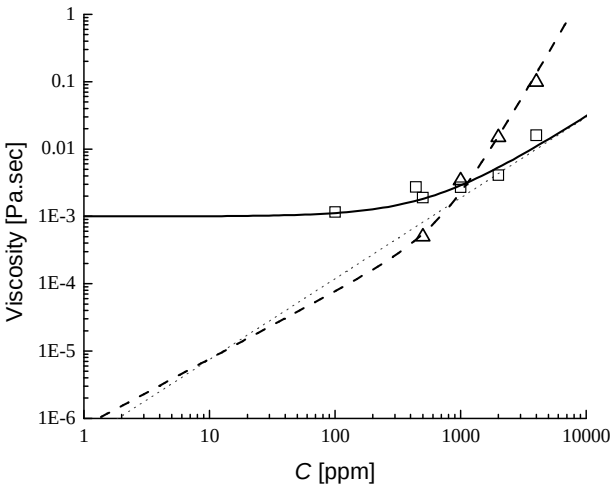

FIGURE 1. Solvent viscosity η_s and polymer viscosity η_p as a function of the concentration of polymer molecules. Experimental data (*WSR301 MI series*) were obtained at the low shear region: □, η_s; △, η_p; solid line, equation (2.10); dashed line, equation (2.11); dotted line, $\phi^{1.2}$.

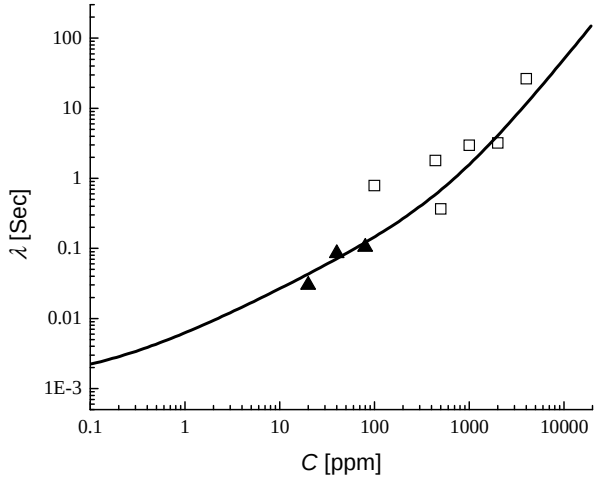

FIGURE 2. Polymer relaxation time λ as a function of the concentration of polymer molecules. □, experimental data (*WSR301 MI series*); ▲, Kalashnikov's data; solid line, equation (2.12).

Then, the friction velocity u_τ can be determined by knowing the wall-shear stress, $\tilde{\tau}_w \equiv \tilde{\tau}_{xy}|_{y=0} = \rho\,\tilde{u}_\tau^2$:

$$\tau_w = \frac{1}{Re}\mathcal{M}_s(\overline{\phi})\frac{\partial U}{\partial y}\Big|_{y=0} + \frac{1}{Re}\frac{\mathcal{M}_p(\overline{\phi})}{We(\overline{\phi})}f\overline{c}_{xy}\Big|_{y=0}\,, \tag{2.19}$$

where the streamwise gradient of mean wall-normal velocity at the wall was neglected because the flow may develop slowly in the x-direction compared to the wall-normal gradient of mean streamwise velocity at the wall. The non-dimensional friction velocity

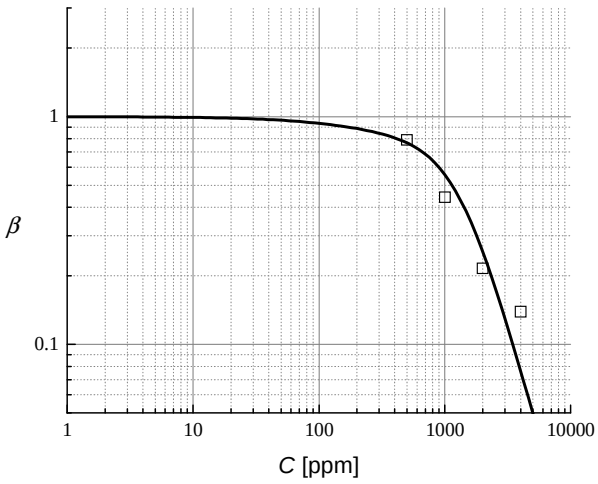

FIGURE 3. The ratio of solvent viscosity to total viscosity, $\beta = \eta_s/(\eta_s + \eta_p)$, as a function of the concentration of polymer molecules. □, experimental data (*WSR301 MI series*); solid line, prediction from (2.10) and (2.11).

is determined by

$$u_\tau = \sqrt{\tau_w}\ . \tag{2.20}$$

The kinematic viscosity of polymeric solution at wall ν_w is defined also from τ_w:

$$\tau_w = \nu_w \left.\frac{\partial U}{\partial y}\right|_{y=0}\ . \tag{2.21}$$

In the viscoelastic turbulent flows, u_τ and ν_w are used as the wall units for representing small-scale turbulence. The drag reduction (DR) is defined by

$$DR = \left(1 - \frac{\tau_w}{\tau_{w,newt}}\right) \times 100\,(\%)\,, \tag{2.22}$$

where $\tau_{w,newt}$ represents the wall-shear stress given from a Newtonian turbulent boundary layer flow.

3. Direct numerical simulations

Here, in the first 3 subsections, briefly summarized is the information about the schemes for the spatial discretizations and the time integration, the boundary conditions for the governing equations, and the simulation conditions (Re_θ, polymer parameters, and so on) for the inhomogeneous-concentration, viscoelastic turbulent boundary layer flows. Subsection 4 is devoted to the simulation results and discussions.

3.1. *Numerical methods*

The governing equations are discretized in space by a finite-volume method on a staggered grid. In (2.5)–(2.9), the velocity field is discretized on the grid cell edges, whereas pressure, conformation tensor and concentration are located on the cell centers. All derivatives involving velocity and pressure are computed through second-order central difference schemes. A third-order Quick scheme is used for the derivatives in the polymer

concentration equation (2.9). A fourth-order compact difference scheme is used for the divergence of the polymer stress tensor in (2.6). The convection term of the polymer conformation tensor is computed using a modified compact upwind difference scheme with third-order accuracy (Min *et al.* 2001) in conjunction with local artificial dissipation (LAD), which is added in any locations where the conformation tensor losses positive definiteness:

$$\frac{\partial}{\partial x_k}\left(u_k c_{ij}\right) \simeq \frac{\partial_u}{\partial x_k}\left(u_k c_{ij}\right) + \kappa {\Delta_k}^2 \frac{{\partial_c}^2}{\partial {x_k}^2}\left(c_{ij}\right)$$

where the operators $\partial_u(\cdot)/\partial x_k$ and $\partial_c(\cdot)/\partial x_k$ denote the upwind-compact and central difference schemes respectively, κ is the coefficient for LAD, and Δ_k the grid mesh in the x_k direction. For any location with $det\{c_{ij}\} \leq 0$, the coefficient κ becomes a non-zero constant (Min *et al.* 2001; Dubief & Lele 2001; Dimitropoulos *et al.* 2005). In the present work, $\kappa = 1$ at the point where c_{ij} loses positive definiteness.

To simulate the turbulent boundary-layer flows that are spatially developing in the streamwise direction, there must be time-dependent turbulent inflow conditions generated on the inlet plane. The inflow database is provided by conducting an additional simulation of Newtonian turbulent boundary layer flow and by saving the time-varying velocity distributions on a cross-sectional surface located in the mid of the domain at which the Reynolds number is maintained around at a value required for the present viscoelastic simulations. The inflow velocity profiles needed in the Newtonian simulation are produced by recycling a velocity plane taken from a downstream position (Lund *et al.* 1998).

The time-integration scheme is a second-order iterative, semi-implicit fractional step method (Pierce & Moin 2004). This scheme can range from iterative explicit to iterative implicit depending on the level of approximation of the Jacobian. The viscous terms of the momentum equation and the diffusion term of the concentration equation in the wall-normal direction are advanced implicitly, whereas all other terms are integrated explicitly. In the conformation equations, all terms are integrated explicitly, except for the spring force term, which is treated implicitly. The time-integration scheme utilizes a multi-grid solver for the Poisson equation for the pressure to apply the incompressibility constraint at every iteration for each time step. The multi-grid solver is used for the planes perpendicular to the spanwise direction, and the Fourier transform is taken in the spanwise direction (Pierce 2001).

3.2. *Boundary conditions*

For the momentum equations, the inflow condition is prescribed at the inlet by using the inflow database generated and the no-slip boundary condition at the wall ($y = 0$). At the free-stream ($y = L_y$, top boundary), Neumann boundary conditions are applied for the streamwise (x) and spanwise (z) velocity components. And the outflow boundary condition is applied for the wall-normal component, v, which is consistent with the boundary layer growth:

$$\left.\frac{\partial u}{\partial y}\right|_{y=L_y} = \left.\frac{\partial w}{\partial y}\right|_{y=L_y} = 0\,, \quad v\big|_{y=L_y} = U_{fs}\left.\frac{\partial \delta^*(x)}{\partial x}\right|_{y=L_y},$$

where δ^* denotes the displacement thickness. At the outlet plane ($x = L_x$), a convective boundary condition is applied:

$$\left(\frac{\partial \boldsymbol{u}}{\partial t} + U_c \frac{\partial \boldsymbol{u}}{\partial x}\right)_{x=L_x} = 0\,,$$

where U_c is the local bulk velocity. In the spanwise direction, periodic boundary conditions are used.

For the conformation equation, one-sided conservative compact difference schemes are used on the free-stream (top) boundary, the wall (bottom) boundary, and the outlet. Periodic boundary conditions are used in the spanwise direction. At the inlet ($x = 0$) the conformation tensor is set to have equilibrium value in order to see the evolution of polymer stretching.

Finally, for the polymer concentration, Neumann boundary conditions are used on the free-stream boundary, the wall boundary, and the outlet. Periodic boundary conditions are used in the spanwise direction. In order to consider the polymer injection at the inlet, the concentration profile is prescribed at the inlet plane in the wall-normal direction:

$$\phi(y)_{x=0} = \phi_{max} \frac{1}{1 + \exp\{(y - \mathcal{X})/\delta\mathcal{X}\}}, \tag{3.1}$$

where the functional shape of the profile was given from a separate simulation of the injector part by utilizing RANS (v^2-f-p) model, which is now being developed by the Stanford drag reduction group. In (3.1), ϕ_{max}, $\mathcal{X}$ and $\delta\mathcal{X}$ are set to fit the prediction from the RANS simulation: $\mathcal{X} = 0.12$ and $\delta\mathcal{X} = 0.025$, which may be effective only in the region of $y^+ \lesssim 10$. To see the effect of concentration thickness, we also tested the additional inlet profile, which is effective in $y^+ \lesssim 20$: $\mathcal{X} = 0.2$ and $\delta\mathcal{X} = 0.05$

3.3. *Simulation conditions*

The Reynolds number based on the momentum thickness, Re_θ, is around 800 at the inlet station. The viscosity of pure solvent is specified as $\eta_{s0} = 6\times10^{-4}$ in computational units. The free stream velocity at $y = L_y$ is $U_{fs} = 1$. At the inlet position, the friction velocity is $u_\tau = 0.049$, the momentum thickness is $\theta = 0.48$, the displacement thickness is $\delta^* = 0.71$, and the boundary layer thickness is $\delta = 4.45$ (in computational units). The domain size ($L_x \times L_y \times L_z$) for the viscoelastic turbulent boundary flows is $17.1\delta_{in} \times 2.6\delta_{in} \times 1.7\delta_{in}$, where δ_{in} denotes δ at inlet, and the mesh size is $256 \times 64 \times 64$, in the streamwise, wall-normal and spanwise directions, respectively. The mesh spacing scaled with wall units (u_τ and ν_w) at inlet is $\Delta x^+ = 24.2$, $\Delta y^+ = 0.74 \sim 39.6$, and $\Delta z^+ = 9.7$. Total time interval for the simulations is $3300\,\theta_{in}/U_{fs}$, which may be long enough to get a stationary state of flow statistics.

The parameters for the polymer molecules are specified as follows. The maximum extensibility (L) of polymer molecules modelled as FENE-P dumbbell spring is chosen to be 100, and the Weissenberg number based on Zimm time and the turbulent shear rate, $We_{\tau,0} \equiv \lambda_0 {u_\tau}^2/\eta_{s0}$, is 0.71. $We_{\tau,0} = 0.71$ corresponds to $We_0 \equiv \lambda_0 U_{fs}/l_c = 0.177$ when we set $l_c = 1$ in a computational unit. In the present work, the Schmidt number Sc of polymer molecules is set to be 1 for convenience. Since the molecular weight of polymer is generally too high, we may need to consider a high Sc of around $O(10^5)$. This may lead to a high-resolution computation to resolve the behavior of small-scale concentration, since the highest wavenumber necessary varies with $Sc^{1/2}$ (Batchelor 1959). The smallest scale at $Sc \sim O(10^5)$ may not be resolved by using the present computational mesh.

In the present work, three different simulations were conducted, and the primary parameters for the simulations are summarized in Table 1.

	Case 1	Case 2	Case 3
ϕ_{max}	0.847	1.695	1.695
$\mathcal{X}$	0.12	0.12	0.2
$\delta\mathcal{X}$	0.025	0.025	0.05

TABLE 1. Simulation cases for $Re_\theta = 800$, $L^2 = 10000$ and $We_{\tau,0} = 0.71$.

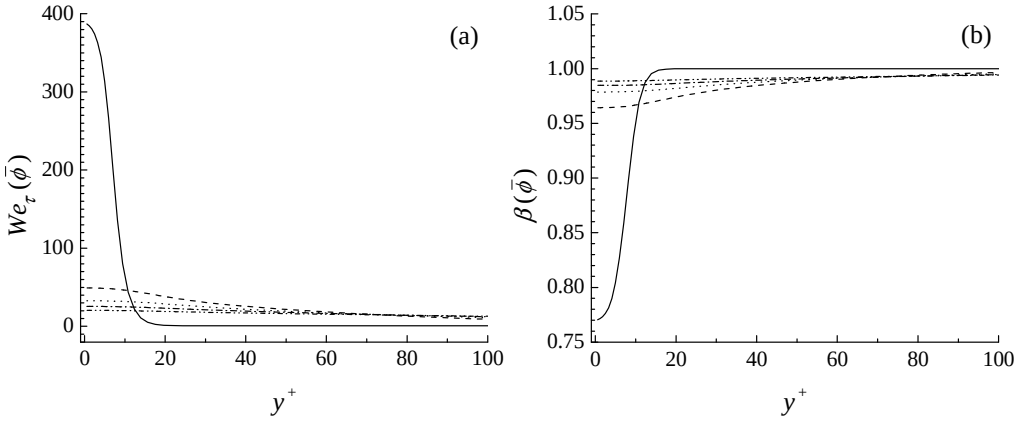

FIGURE 4. Wall-normal distributions of (a) $We_\tau(\overline{\phi})$ and (b) $\beta(\overline{\phi})$ at various downstream positions for Case 1: solid line, $x = 0$; dashed line, $x = 3.4\delta_{in}$; dotted line, $6.8\delta_{in}$; dash-dotted line, $10.2\delta_{in}$; dash-dot-dotted line, $13.6\delta_{in}$.

3.4. *Results and discussion*

3.4.1. *Overview*

The near-wall turbulence structure may be retained by the mechanisms of high-speed sweep and low-speed ejection, and the vortical motions in the near wall region may be closely related to the production of turbulence in the boundary layer (Robinson 1991). By injecting the polymer molecules, the near-wall vortical motions are dampened in following downstream, and, thereby, the drag on the wall may be modified. Polymers are stretched rapidly in the upstream region close to the inflow plane, and the stretched polymers may produce a large stress somewhere else in the boundary layer. This stress may contribute to the suppression of turbulence in the downstream, and, finally, may lead to the reduction of drag.

3.4.2. *Transit time and polymer shear viscosity*

To explain the mechanism of drag reduction in the viscoelastic turbulent boundary layer with near-wall injection of polymer molecules, two important parameters of transit time and polymer shear viscosity are introduced in this work. As shall be described in the following, these two parameters are related mostly to the flow characteristics in viscous-wall region $y^+ < 50$, where a molecular viscosity may have direct influence on the shear stress. It should be noted in advance that the polymer shear viscosity is a molecular property.

In the present work, the polymer concentration ϕ is spatially non-uniform throughout

the domain so that the rheological parameters of η_s, η_p and λ vary with position and time. Figure 4 represents the wall-normal distributions of We_τ and β, which are averaged in spanwise direction at various downstream positions for Case 1. Since the polymer concentration decreases along the streamwise direction as it is rapidly dispersed out from the wall, the peak value of We_τ decreases from around 400 at the inlet to 50 at $x = 3.42\delta_{in}$ and 20 at $x = 13.6\delta_{in}$. This implies that in the downstream, the transition of stretched polymers near the wall to a coiled state may occur so rapidly that the polymers lose the elastic energy that is gained from near wall region before they reach the buffer layer ($y^+ \geq 30$). Similarly but oppositely, the peak value of β, which is the ratio of solvent viscosity to total viscosity, increases quickly from 0.77 at inlet to 0.96 at $x = 3.42\delta_{in}$. For $x > 7\delta_{in}$, the viscosity ratio β remains a large value of around 0.98 and, therefore, the contribution of polymer stress (represented by $1 - \beta$) to the total shear stress becomes small in the downstream.

Let us define a "transit time" T_{tr} during which a polymer initially located at a certain position of $y^+ \simeq \delta_c^+$ in the near-wall region travels to buffer region $y^+ \geq 30$:

$$T_{tr}^+ = \int_{y^+ \simeq \delta_c^+}^{y^+ \simeq 30} \frac{y^+}{\nu_{turb}^+}\, dy^+ , \tag{3.2}$$

where δ_c denotes the characteristic position of a parcel of polymer molecules suffering from strong extensional flows and

$$\nu_{turb} = -\overline{u'v'}\left(\frac{\partial U}{\partial y}\right)^{-1}$$

is the eddy viscosity. In Case 1 ($\delta_c^+ \simeq 10$), T_{tr}^+ varies between 130 to 350, depending on the streamwise position. Comparing We_τ with T_{tr}^+ and considering the rapid decay of ϕ in the streamwise direction, the drag may be reduced mainly by the polymers stretched at a near-inlet region, where We_τ remains around 200 and the polymer may have enough time to travel to the buffer region while maintaining a certain amount of stretching. If the polymer molecules are injected around the buffer layer, the transit time of polymer molecules at the inlet position may be irrelevant to the onset of drag reduction and to the modification of the near-wall structure of turbulence. In this case, the initial onset of drag reduction may be triggered mainly by the concentration of polymer molecules itself because the high concentration at the injection position induces a significant increase in the solvent viscosity. The viscous effect due to the high concentration of polymer molecules at the inlet may be followed by the viscous dissipation induced by the polymers, which may gain an elastic energy by encountering straining flows around the wall region, and which may then return to the buffer region to release the energy. During that procedure, the drag reduction may begin to depend on the transit time T_{tr} of polymer molecules in the downstream.

The polymer molecules stretched by near-wall straining flows (Terrapon *et al.* 2004) may store elastic energy and may release it during stretch-to-coil transition. Though the stretch-to-coil transition occurred inside the viscous-wall region where there exists the direct effect of molecular viscosity on the shear stress, the energy stored in stretched polymers may be released in the form of dissipation. As can be seen in (2.6), the molecular shear stress is composed of $\tau_{s,xy}$ and $\tau_{p,xy}$:

$$\tau_{s,xy} + \tau_{p,xy} = \frac{\mathcal{M}_s(\phi)}{Re}\frac{\partial u}{\partial y} + \frac{1}{Re}\frac{\mathcal{M}_p(\phi)}{We(\phi)} f c_{xy} .$$

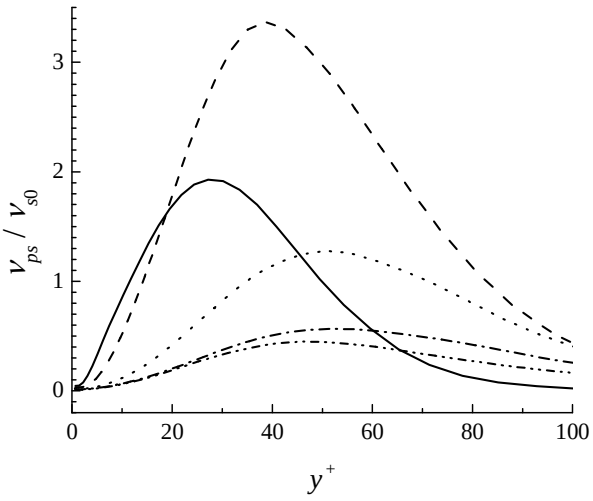

FIGURE 5. Wall-normal distributions of the polymer shear viscosity ν_{ps} induced by the polymer stress at various downstream positions in Case 1, where ν_{s0} is the kinematic viscosity of pure solvent viscosity: solid line, $x = 1.7\delta_{in}$; dashed line, $3.4\delta_{in}$; dotted line, $6.8\delta_{in}$; dash-dotted line, $10.3\delta_{in}$.; dash-dot-dotted line, $13.7\delta_{in}$.

That is, if the concentration of polymer molecules is not diluted and c_{xy} is considerable, the polymer stress $\tau_{p,xy}$ may induce an additional molecular viscosity, which may contribute to the attenuation of a flow inertia, resulting in the diminution of flow instability playing an important role in the generation of coherent vortical motions. This additional viscosity from the polymer shear stress ν_{ps} can be determined by

$$\overline{\tau}_{p,xy} = \nu_{ps} \frac{\partial U}{\partial y} \,. \tag{3.3}$$

From now on, we call ν_{ps} the "polymer shear viscosity". Figure 5 represents the wall-normal distribution of ν_{ps} normalized with the kinematic viscosity of pure solvent viscosity ν_{s0} ($\equiv \eta_{s0}/\rho$) at various downstream positions in Case 1. The polymer shear viscosity develops rapidly with x and becomes comparable with ν_{s0} at early stages of upstream $x = 1.7\delta_{in}$, which is approximately close to a position where DR begins to be positive. For $x > 3.4\delta_{in}$, however, ν_{ps} begins to decay with x. For $x > 6.8\delta_{in}$, ν_{ps} becomes less than ν_{s0}. Strikingly, the position of peak in the wall-normal distribution is located in the buffer layer, and the peak value overwhelms the viscosity of pure solvent ν_{s0} in the upstream region where DR develops. The increased viscosity, $\nu_s + \nu_{ps}$, in the viscous-wall region $y^+ < 50$ may strengthen the viscous dissipation and thereby suppress the inertial effect in the near-wall region (in the case of the near-wall injection of polymers, $\nu_s \simeq \nu_{s0}$ in the buffer region). The decrease of inertial effect may attenuate the vortical motion and prohibit the turbulence cascade in the region of high wave numbers (Tabor & de Gennes 1986). As a result, the polymer shear viscosity that stems from the polymer molecules makes the size of the smallest eddy in near wall region increasingly larger according to the following scaling law:

$$l_K = \left({\nu_m}^3/\epsilon\right)^{1/4},$$

where l_K represents the Kolmogrov length scale, ν_m represents the molecular viscosity

($\nu_m = \nu_s + \nu_{ps}$), and ϵ represents the dissipation rate. The dissipation rate ϵ is usually defined by the balance equation for the turbulent kinetic energy, $k_e \equiv \frac{1}{2}\overline{u_k' u_k'}$:

$$\frac{Dk_e}{Dt} = -\frac{1}{2}\nabla \cdot \overline{\boldsymbol{u}' \cdot \boldsymbol{u}'\boldsymbol{u}'} + \mathcal{P} + \Pi + \epsilon + \nabla \cdot \left(\nu_m \nabla k_e\right),$$

where $\mathcal{P}$ is the production rate and Π is the product of velocity and pressure fluctuations. Since the viscosities of ν_s and ν_{ps} are dissipative quantities, if we assume that their fluctuations may be statistically independent of turbulent fluctuation of velocity vectors or velocity gradient tensors, the viscous dissipation rate of polymeric solution may be expressed as

$$\epsilon = -\nu_s \overline{\nabla \boldsymbol{u}' : \nabla \boldsymbol{u}'^{\top}} - 2\nu_{ps}\, \overline{\boldsymbol{s}' : \boldsymbol{s}'}\,, \tag{3.4}$$

where $\boldsymbol{s}'$ is the fluctuation part of the rate-of-strain tensor $\boldsymbol{S}$. The fluctuation of polymer stress not only contributes to the viscous dissipations but also to the term of the product of velocity and pressure fluctuations:

$$\Pi = -\nabla \cdot (\overline{\boldsymbol{u}' p'}) + \nabla \cdot (\overline{\boldsymbol{u}' \cdot \boldsymbol{\tau}_p'})\,. \tag{3.5}$$

The second terms on the right-hand side of (3.4) and (3.5) represent the contribution of polymer stress to ϵ and Π, respectively. Note that, by definition, the viscous dissipation due to the polymer shear stress is directly proportional to the square of local strain rate (see (3.4)). This implies that the correlation between local straining motion and the fluctuation of polymer shear stress may play an important role in the modification of the energy cascade in (dissipative) small-scale turbulence. In the downstream, as mentioned before, the concentration of polymers becomes very dilute. As the concentration of polymer molecules becomes very dilute, We_τ becomes less than T_{tr}^+ and, at the same time, the contribution of polymer stress decays toward zero. Therefore, the viscous dissipation associated with the polymer shear viscosity ν_{ps} decreases with x in the region downstream of $x > 4\delta_{in}$.

3.4.3. *Polymer stretching*

Figure 6 is the plot for (a) the streamwise variations of mean concentration $\overline{\phi}$ and trace of conformation tensor c_{kk} at the wall and (b) the wall-normal distribution of c_{ij} ($i, j = x$ or y) at various downstream positions for Case 1. The injected polymers may not penetrate into the downstream effectively, in such a way that ϕ at the wall decays to below 10% of C^*, even at $x \simeq 4\delta_{in}$. The decay of polymer stretching is almost in phase with that of polymer concentration. Even though c_{ij} is specified to be a coiled state at the inlet, c_{ij} develops quickly by the strong flows containing high-concentration polymers near the inlet and decays in the downstream. The polymer stretch of c_{xx} has a peak value at around $y^+ \simeq 10$. On the other hand, c_{xy} has a peak value on the edge of the buffer layer $y^+ \simeq 30$, and the peak value of c_{yy} is located in the mid of the buffer layer $y^+ \simeq 50$. Near the wall, the stretched polymer is more likely to be aligned with the quasi-streamwise vortices. In the buffer layer, where there exist vortical motions associated with the motions of sweep and ejection, the polymers may be partially aligned with the axes of hairpin vortices. Since the buffer region may be a region where the polymers release elastic energy (Min *et al.* 2003), c_{xy} is dominant in this region and may contribute to a molecular dissipation of polymeric fluid.

3.4.4. *Drag reduction*

In the present simulations, the near-wall injection of polymer molecules leads to the drag reduction (DR) of around 40% for Case 1, Case 2 and Case 3 independently of the

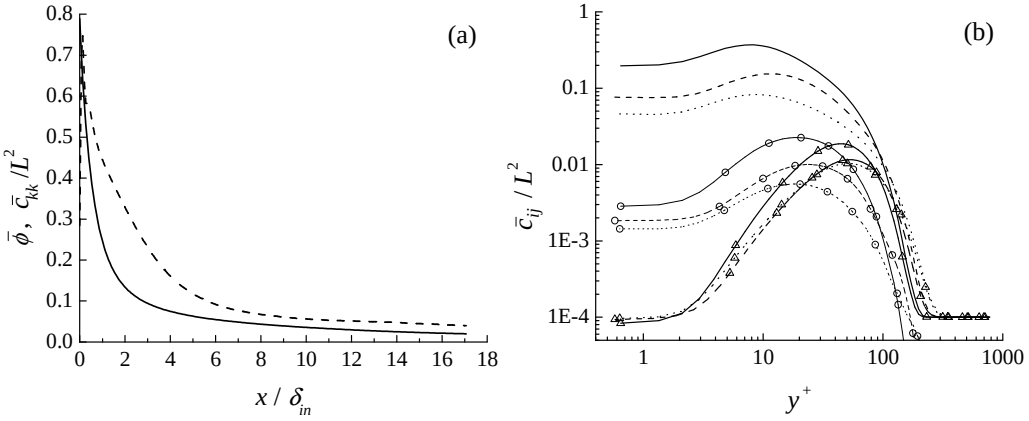

FIGURE 6. Streamwise variations of (a) mean concentration (solid line) and polymer stretching (dashed line) at the wall and (b) wall-normal distribution of c_{ij} at various downstream positions for Case 1. In (b), solid, dashed and dotted lines indicate the downstream positions of $x = 3.4\delta_{in}$, $6.8\delta_{in}$ and $13.7\delta_{in}$, respectively: lines without symbol, c_{xx}; lines with $\circ$, c_{xy}; lines with $\triangle$, c_{yy}.

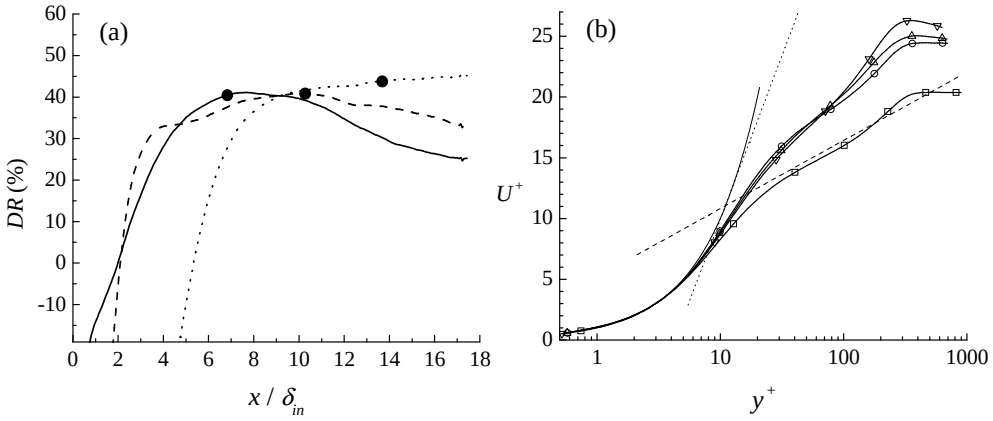

FIGURE 7. (a) Streamwise variation of drag reductions predicted by the simulations: solid line, Case 1; dashed line, Case 2; dotted line, Case 3. Marks of black circles in DR curves indicate the streamwise positions of $6.8\delta_{in}$, $10.2\delta_{in}$, and $13.7\delta_{in}$, respectively. (b) Mean streamwise velocities at the marked positions in (a). Lines with symbols are the simulations: line with $\square$, Newtonian; line with $\circ$, Case 1 ($x = 6.8\delta_{in}$); line with $\triangle$, Case 2 ($10.2\delta_{in}$); line with $\triangledown$, Case 3 ($13.7\delta_{in}$). Lines without symbol are asymptotes: solid line, $U^+ = y^+$; dashed line, equation (3.6); dotted line, equation (3.7).

amount of polymers injected (see Fig. 7). Since the polymer concentration is highest at the inlet position, the inflow faces a flow region where η_s is $1.8\eta_{s0}$ in Case 1 or $2.9\eta_{s0}$ in Case 2 and Case 3. This abrupt increase of solvent viscosity leads to an increase of shear stress at the wall, resulting in a huge increase of drag near the inflow plane. However, simultaneously, the polymer molecules may absorb huge elastic energy in this region, and they may penetrate into the buffer layer to release their energy ($We_\tau > T_{tr}^+$). Surrounding turbulence becomes suppressed probably by the increase of viscous dissipation due to

the direct increase of molecular viscosity η_s and to the energy release from the polymer molecules, and thereby the vortical motion is dampened in the downstream. During this procedure, the drag reduction increases with x and reaches a peak value of around 40%. The polymer molecules injected at the inlet spread out rapidly from the near wall, and the decrease in the amount of polymers leads to the decrease of polymer relaxation time We_τ. The extremely diluted polymers in the downstream may not contribute to the suppression of turbulence effectively, because their relaxation time is too small to reach the buffer layer ($We_\tau \ll T_{tr}^+$) in a stretched state that is strong enough to induce a significant impact on $\tau_{p,xy}$. Therefore, the drag reduction may keep decreasing from the peak in the downstream region. In Case 3 ($\phi_{max} = 1.695$, $\delta_c^+ \simeq 20$), the total amount of polymer molecules injected is around twice that of Case 2, and T_{tr} is decreased due to the increase in concentration thickness. The turbulence modified by the stretched polymers near the inflow plane may be retarded due to influence of the turbulence in the downstream, so that the drag reduction is continuously developing in the domain.

Figure 7(b) represents the typical profile of mean streamwise velocity in the region of drag reduction. In Case 1, the velocity profile in the log-law layer is shifted up without changing the slope, which is typical in low-drag-reduction (LDR) regimes. As the total amount of polymers increases (Case 2 and Case 3), the slope is changed, which is typical in high-drag-reduction (HDR) regimes. These velocity profiles of simulated viscoelastic turbulent boundary layer were also compared with Newtonian log-law,

$$U^+ = 2.5 \ln y^+ + 5.5\,, \tag{3.6}$$

and with Virk's (1971) asymptote for the maximum-drag-reduction (MDR),

$$U^+ = 11.7 \ln y^+ - 17\,. \tag{3.7}$$

The comparison shows that the slope in the log-law region increases and approaches Virk's asymptote as the amount of polymers injected increases. However, it should be noted that Virk's experiment was conducted for the pipe flows at high Reynolds number ($Re_b > 10000$, b the pipe radius), while the present study is for the turbulent boundary layer flows in low-Reynolds number ($Re_b \sim Re_\delta \simeq 5900$). To see the MDR asymptote in the turbulent boundary layer, a larger grid system may be required to resolve properly the small-scale turbulence at higher Reynolds numbers (Min *et al.* 2003).

3.4.5. *Flow statistics*

Figure 8 is the plot for the r.m.s. streamwise and wall-normal velocity fluctuations normalized (a) with large scale quantities and (b) with small-scale quantities such as wall units, for Case 1. When DR develops (e.g. $x = 3.4\delta_{in}$), the levels of u_{rms} and v_{rms} are dampened, and it is apparent that the peak position of v_{rms} is shifted away from the wall. However, u_{rms} keeps increasing to the level of Newtonian one until DR reaches a peak value and remains at that level. v_{rms} decreases initially with x but may regress to the level of the Newtonian as DR decreases with x in the downstream. On the scaling with wall units such as u_τ and ν_w, it is clearly seen that v_{rms}^+ inside the viscous-wall region $y^+ < 50$ is smaller than that of the Newtonian in upstream but v_{rms}^+ is increased and probably goes back to the Newtonian level as the concentration of polymer molecules becomes lower with x. Therefore the near-wall polymers may not contribute to the turbulence modification because We_τ becomes much less than T_{tr}^+ there, and the polymer shear dissipation around the buffer layer, which may be induced by the polymer stress, becomes weakened in the downstream.

Finally, the shear stress and the wall-normal polymer force at various downstream

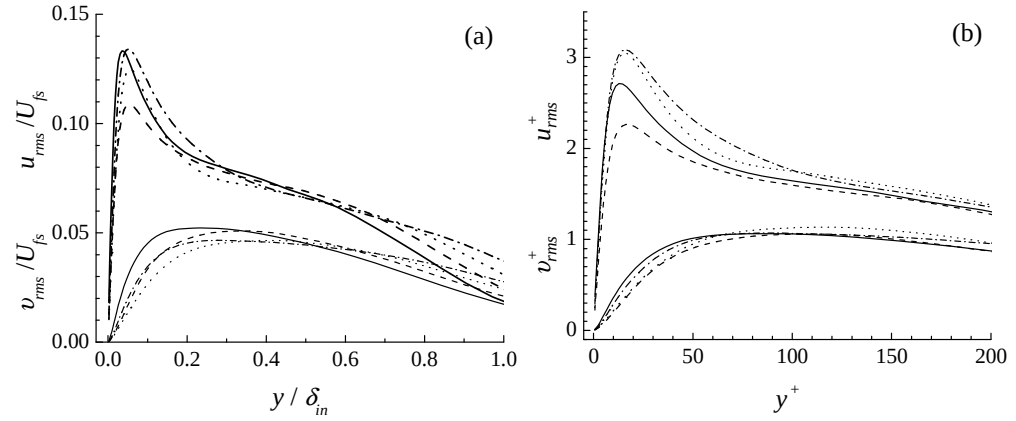

FIGURE 8. The rms values of u' and v' normalized with (a) large scale quantities and (b) wall units at various downstream positions in Case 1: solid line, Newtonian; dashed line, $x = 3.4\delta_{in}$; dotted line, $6.8\delta_{in}$; dash-dotted line, $13.7\delta_{in}$.

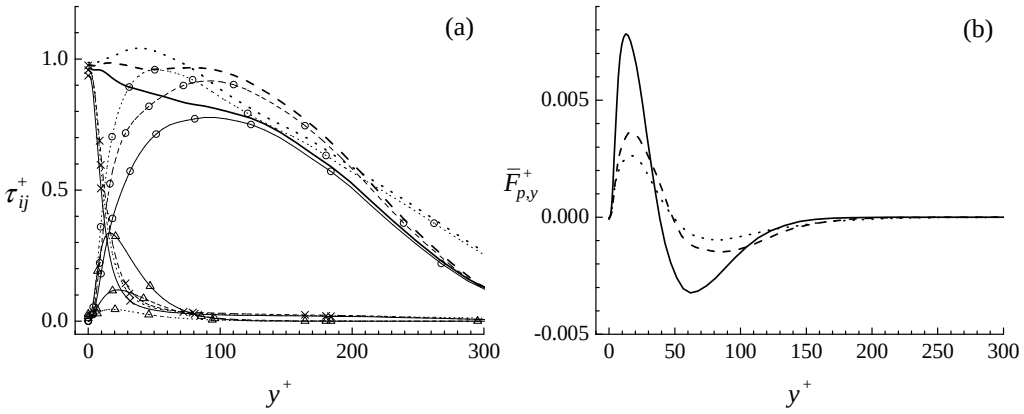

FIGURE 9. Wall-normal distributions of (a) shear stress and (b) polymer force in the y-direction at various downstream positions in in Case 1. Downstream position is indicated by lines: solid line, $x = 3.4\delta_{in}$; dashed line, $6.8\delta_{in}$; dotted line, $13.7\delta_{in}$. Lines without symbol in (a) represent the total shear stress, τ^+_{xy}. Symbols indicate the type of shear stress: lines with $\circ$, $-\overline{u'^+v'^+}$; lines with $\times$, $\overline{\tau}^+_{s,xy}$; lines with $\triangle$, $\overline{\tau}^+_{p,xy}$.

positions (Case 1) are plotted in Fig. 9. By the injection of polymer molecules, the Reynolds stress $-\overline{u'v'}$ increases near the inflow plane and then immediately decreases until the polymer concentration becomes dilute enough such that We_τ is less than the transit time T^+_{tr}. For Case 1, $-\overline{u'v'}$ decreases with x in $x \lesssim 4\delta_{in}$ and increases slowly after that. This behavior may not be seen in the wall-unit scaling. Under the wall-unit scaling, we can compare the contributions of various shear components to the total shear stress. The mean polymer shear stress $\overline{\tau}^+_{p,xy}$ has maximum value at very near the inflow plane. Along the streamwise direction, $\overline{\tau}^+_{p,xy}$ weakens because the near-wall region loses polymer molecules and We_τ decreases. On the other hand, the Reynolds stress (which is decreased initially) recovers toward the level of the Newtonian as the polymer effect

weakens. Since the polymer stress decreases along with the streamwise direction, the polymer force $\boldsymbol{F}_p = \nabla \cdot \boldsymbol{\tau}_p$ acting on the solution fluid also decreases. The wall-normal component of mean polymer force, $\overline{F}_{p,y}$, is positive in $y^+ < 40 \sim 50$ but negative in the buffer layer. The stretched polymers accelerate low-speed fluid away from the wall in $y^+ < 40 \sim 50$ and pull back the fluid in $y^+ > 40 \sim 50$. The wall-normal polymer force may contribute to the upward shift of mean streamwise velocity in the buffer layer.

4. Future plans

In this work, the computational method to consider the viscoelastic turbulent boundary layer flows containing spatially inhomogeneous concentration of polymer molecules was developed, and the concentration-dependent rheological parameters were taken into account in the simulations. In order to explain the drag-reduction mechanism in the inhomogeneous concentration viscoelastic turbulent boundary layer flows, a time scale of the transit time of near-wall polymers (T_{tr}) and an additional parameter of the polymer shear viscosity (ν_{ps}) were introduced and were used in the investigation of the interaction between turbulence and non-uniformly distributed polymer molecules. It was found that these two parameters are not only useful to explain the mechanism of drag reduction but are also consistent with the insights to the mechanism provided previously by Lumley (1969), Tabor & de Gennes (1986) and Joseph (1990). The previous insights to the mechanism of turbulent drag reduction may be partly correct but, at the same time, partly incomplete. Additionally, it was found that the polymer molecules contribute to the viscous dissipation of turbulent kinetic energy of the solution phase and, particularly, that this additional viscous dissipation is independent of the rotational motion but is related only to the local straining motion of fluid. The authors hope that the parameters of T_{tr} and ν_{ps} and the existence of an additional viscous dissipation due to the polymer molecules, newly presented through this work, will be useful to combine the existing hypotheses for the drag-reduction mechanism and, moreover, will give a complete answer to this long-pending question.

There are several issues in the grid resolution for the present preliminary simulations. The present simulations for $Re_\theta = 800$ used relatively small grid system of $17.1\delta \times 2.6\delta \times 1.7\delta$ for convenience. To properly resolve the turbulence characteristics in the spanwise direction, the domain width in that direction should be larger than at least 3.5δ, within which the spanwise two-point velocity correlation decays out (Min *et al.*, 2003). $L_z = 7\delta$ (around double of a length scale associated with the velocity correlation) may be a proper choice in the future simulations. The near-wall injection of polymer molecules may induce sharp gradients of polymer conformation tensor near the wall in the wall-normal direction. Even though the present grid resolution in y-direction would be enough to consider the velocity field, there may be a need to consider a finer mesh inside the viscous sublayer in order to resolve the sharp gradients of polymer stress tensor near the wall. By utilizing a finer grid system, we will investigate the following questions in the future study: (i) how does the turbulence respond to the injection of polymer molecules?; (ii) what is the relation between the transit time and the elastic theory in the drag-reduction mechanism?; (iii) is it true that the polymer shear viscosity in the viscous-wall region attenuates the flow inertia and thereby modifies the energy cascade in the high-wavenumber region?; (iv) can we get HDR and MDR by the near-wall injection of polymers and, if yes, is there any unique feature in those regimes for the turbulent boundary layer flows?

Acknowledgment

The support of DARPA (Grant No.: MDA972-03-1-0033) is acknowledged.

REFERENCES

Batchelor, G.K. 1959 Small-scale variation of convected quantities like temperature in turbulent fluid. part 1. general discussion and the case of small conductivity. *J. Fluid Mech.* **5**, 113–133.

Lumley, J.L. 1969 Drag reduction by additives. *Ann. Rev. Fluid Mech.* **1**, 367–384.

Lumley, J.L. 1973 Drag reduction in turbulent flow by polymer additives. *J. Poly. Sci. Mac. Rev.* **7**, 263–290.

Lund, T. S., Wu, X. & Squires, K. D. 1998 Generation of turbulent inflow data for spatially-developing boundary layer simulations. *J. Comp. Phys.* **140**, 233–258.

Dimitropoulos, C. D., Dubief, Y., Shaqfeh, S. G., Moin, P. & Lele, S. K. 2005 Direct numerical simulation of polymer-induced drag reduction in turbulent boundary layer. *Phys. Fluids* **17**, 0117050-1–0117050-4.

Dubief, Y. & Lele, S. K. 2001 Direct numerical simulation of polymer flow. *Annual Research Briefs 2001*, Center for Turbulence Research, NASA Ames/Stanford Univ., 197–208.

Dubief, Y., White, C. M., Terrapon, V. E., Shaqfeh, S. G., Moin, P. & Lele, S. K. 2004 On the coherent drag-reducing and turbulence-enhancing behavior of polymers in wall flows. *J. Fluid Mech.* **514**, 271–280.

Joseph, D. D. 1990 *Fluid Dynamics of Viscoelastic Liquids*. Springer.

Min, T. & Choi, H. 2001 Effect of spatial discretization schemes on numerical solutions of viscoelastic fluid flows. *J. Non-Newtonian Fluid Mech.* **100**, 27–47.

Min, T., Choi, H., & Joseph, D. D. 2003 Drag reduction by polymer additives in a turbulent channel flow. *J. Fluid Mech.* **486**, 213–238.

Pierce, C. 2001 A progress-variable approach for large-eddy simulation of turbulent combustion. *Ph.D. Thesis*, Stanford University.

Robinson, S. 1991 Coherent motions in the turbulent boundary layers. *Ann. Rev. Fluid* **23**, 601–639.

Sureshkumar, R., Beris, A. N. & Handler, R. A. 1997 Direct numerical simulation of the turbulent channel flow of polymer solution. *Phys. Fluids* **9**, 743–755.

Tabor, M. & de Gennes, P. G. 1986 A cascade theory of drag reduction. *Europhys. Lett.* **2**, 519–522.

Terrapon, V. E., Dubief, Y., Moin, P., Shaqfeh, S. G., & Lele, S. K. 2004 Simulated polymer stretch in a turbulent flow using Brownian dynamics. *J. Fluid Mech.* **504**, 61–71.

Toms, B. A. 1948 Some observations on the flow of linear polymer solutions through straight tubes at large Reynolds numbers. *Proc. 1st Intl. Congress on Rheology* **2**, 135–141.

Virk, P.S. 1971 An elastic sublayer for drag reduction by dilute solutions of linear macromolecules. *J. Fluid Mech.* **337**, 193–231.